Third International Symposium on Marine Propulsors
smp'13, Launceston, Tasmania, Australia, May 2013

Numerical and Physical Investigation of a Surface-Piercing Hydrofoil

Yin Lu Young[1], Stefano Brizzolara[2]

[1] Dept. of Naval Architecture and Marine Engineering, University of Michigan, Ann Arbor, MI, 48109, USA, ylyoung@umich.edu
[2]Dept. of Mechanical Engineering, Sea Grant AxV Design Lab, MIT, Cambridge, MA, 02139, USA, stebriz@mit.edu

ABSTRACT

The objective of this work is to extend a 3-D boundary element method for modeling the hydrodynamic response of a surface-piercing hydrofoil with consideration for the effects of cavitation and/or ventilation. The problem is formulated as a mixed boundary value problem for the perturbation velocity potential. The effect of the submerged depth based Froude number and ventilation on the cavity pressure is considered. The numerical predictions are compared with experimental measurements conducted at a free surface cavitation tunnel. The results show good comparisons between experimental measurements and numerical predictions in the base cavitating regime, when the cavity is closed to the free surface. When the cavity is open to the free surface, the pressure in the ventilated cavity, P_c, varies between the vapor pressure (P_v) and the absolute ambient pressure (P_∞) depending on the angle of attack, submergence, relative inflow velocity, difference between P_∞ and P_v, and is influenced by hysteresis effects. Consequently, the lift coefficients vary significantly. The upper limit of the measured lift coefficients matched well with numerical predictions for $P_c=P_v$ (fully attached or base cavitating regime), and the lower limit matched well with numerical predictions for $P_c=P_\infty$ (fully ventilated regime at very high Froude number and very low absolute ambient pressure).

Keywords

Surface-piercing, ventilation, cavitation, hydrofoil

1 INTRODUCTION

Streamlined surface-piercing (SP) bodies such as hydrofoils, struts, rudders, propeller blades, etc, are often used to support or propel high-speed vessels. Since SP bodies intercept the free surface, they may be subject to cavitation and/or ventilation depending on the operating condition. Cavitation is simply identified here as when the local absolute pressure drops to the saturated liquid vapor pressure, and ventilation is defined as the entrainment of air from the atmosphere to the submerged portion of the body. Previous work (Scherer & Auslaender, 1965; Young & Kinnas, 2004; Brizzolara & Young, 2012) has shown that there exist four major flow regimes for a surface-piercing body:

1. ***Fully Attached (FA)*** – where both the suction and pressure sides of the foil are fully wetted. If the foil has a thick trailing edge, a separated region will form behind the trailing edge. If the pressure in the separated region is equal to the saturated liquid vapor pressure, the flow is called *based cavitating*. If the pressure in the separated region is equal to the ambient atmospheric pressure, the flow is called *based ventilated*.
2. ***Transitional (TR)*** – where mixed cavitation and/or ventilation patterns develop on the foil surface. The flow is very unstable with large load fluctuations.
3. ***Supercavitating (SC) or Fully Ventilated (FV)*** – where the length of the cavity exceeds the chord length of the foil. If the cavity is closed to the free surface, the flow is called supercavitating; if the cavity is open to the free surface, the flow is called superventilated or fully ventilated.

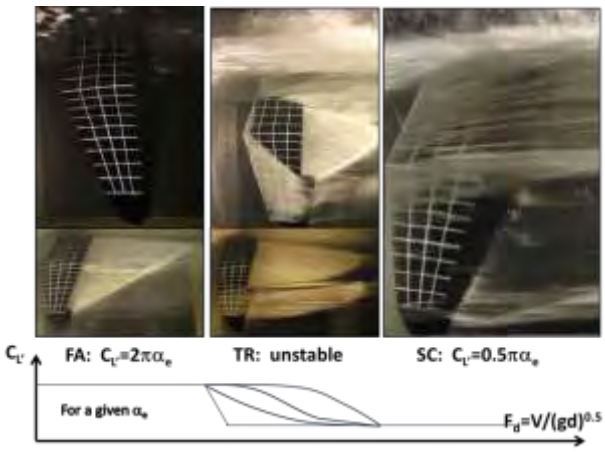

Fig. 1: Variation of flow patterns and lift coefficients in the fully attached (FA), transitional (TR), and fully ventilated (FV) flow regimes.

Sample illustrations of the flow pattern in the three major flow regimes are shown in Fig. 1. In 2-D, the slope of the ideal lift coefficient ($C_{L'}$) versus the effective angle of attack (α_e) curve is equal to 2π in the FA regime, and is equal to $\pi/2$ in the SC regime. In the TR regime, the flow is unstable with partial or mixed cavitation and

ventilation, and may become fully ventilated suddenly. As discussed in Wadlin (1958,1959), Breslin & Skalak (1959), Waid (1968), and Swales et al. (1974), in the case of vertical SP struts/hydrofoils, low pressure is not a sufficient condition for ventilation, but the rupture of the surface 'seal' is needed to admit air. In the absence of free surface disturbance, the flow does not separate at the free surface for low to moderate angles of attack because the longitudinal pressure gradient is zero. As shown in the left and middle pictures on the bottom of Fig. 1, there is a thin layer of water that separates the closed, vaporous cavity below and the free surface above. Once the surface 'seal' is ruptured due to very large angles of attack, free surface disturbances (e.g. waves, debris, seaweed, body motion, wake of adjacent body, etc.), and/or aeration of vortex cores (formed by leading edge vortex, trailing edge vortex, tip vortex, unsteady cavity trailing edge, and/or turbulent flow in the separated region), the flow will become fully ventilated very rapidly as the free surface is drawn down by the suction in the low pressure cavity or vortex core, which will in turn lead to more perturbations, and hence air paths for ventilation. The top picture in the middle of Fig. 1 illustrates a time instance when the surface 'seal' is broken due to increases in angle of attack, and air is being drawn down from the free surface. Once the surface seal is broken, the cavity will grow explosively due to rapid increases in the cavity pressure (from around 2-3 kPa to 101 kPa), as illustrated in the rightmost picture in Fig. 1. Consequently, the lift will drop suddenly and dramatically, and the side force (and twist moment) may reverse in sign (Waid, 1968; Swales et al. 1974). Once the flow reaches a stable FV pattern, the hydrodynamic lift coefficient will stabilize and follow the lower curve shown in Fig. 1, for which the ideal 2-D lift coefficient increases with $0.5\pi\alpha_e$. For high-speed SP hydrofoils/struts, the design operating condition is in the SC/FV regime, which is stable with minimum viscous drag. However, the foil must be able to successfully transition from the FA to the SC/FV regime. For thin, flexible streamlined SP hydrofoils, the sudden load change in the TR regime may lead to structural strength and stability issues, and may affect vessel stability. Hence, it is important to be able to quantify the performance of SP hydrofoils across the range of flow regimes.

Although some research has been conducted in the past to investigate the performance of SP hydrofoils/struts via experimental modeling (e.g. Breslin & Skalak, 1959; Wadlin, 1958 & 1959; Waid, 1968; Rood & Dailey, 1973; Swales et al. ,1974), much of which was on vertical struts and very limited work has addressed the numerical modeling of SP hydrofoils. As outlined by Brizzolara & Villa (2011), who first used a RANSE finite volume solver with a volume of fluid (VOF) approach to model the three phases flow around a SP super-cavitating/ventilating hydrofoil, the numerically simulation of the performance of a SP hydrofoil is a very challenging problem, because it involves free surface deformations, jet sprays, cavitation and ventilation. It should be noted that most current VOF approaches are not valid for modeling of three-phase mixture that may separate or coalesce. Past studies have shown that ventilation depends on the availability of the air path to the cavity, which requires separation of the boundary layer and rupture of the free surface, or interaction between vortex cores with a disturbed free surface. Hence, the hydrodynamic response of the hydrofoil depends on the Reynolds number (which controls flow separation and formation of eddies), Froude number (which controls the free surface response and the behavior of surface sprays), cavitation number (which controls the maximum pressure difference), and the Weber number (which controls the surface tension effects influencing free surface rupture and thickness of the spray sheet). In addition, the ventilation mechanism depends on the foil geometry, submergence, and angle of attack.

As a first step toward the modeling of the hydrodynamic response a SP hydrofoil, a 3-D boundary element method (BEM) is proposed in this work. In order to predict the performance of the SC hydrofoil using the BEM, it is necessary to know the cavity pressure (P_c) when prescribing the dynamic boundary condition on cavity surfaces. However, contrary to natural cavitation on fully submerged hydrofoils, where $P_c=P_v\approx$2-3 kPa (P_v is the saturated liquid vapor pressure of water), $P_c>P_v$ for a SP hydrofoil when the surface 'seal' is ruptured and air is drawn down from the free surface, or when air is entrained at the submerged tip of the hydrofoil (due to hysteresis effect, as illustrated in the bottom, middle picture in Fig. 1). As shown in the experimental data conducted by Wadlin (1959) at the high-speed towing tank at the NASA Langley Research Center, in general, $P_v<P_c<P_{atm}$, where P_{atm} is the atmospheric pressure. Except at very high speed, high angle of attack, and very shallow submergence, $P_c<P_{atm}$ because of the non-zero air flow rate from the free surface to the cavity. Hence, P_c depends on the Froude number, $F_d=V/(gd)^{0.5}$ because the air flow rate depends on the inflow speed V, depth of submergence d, and the difference between P_{atm} and P_v for a given geometry and angle of attack.

2 NUMERICAL MODEL

In this work, a 3-D BEM method is extended for the analysis of 3-D SP hydrofoils. The BEM was first developed by Kinnas & Fine (1991) for the nonlinear analysis of flow around partially and supercavitating 2-D hydrofoils. It was later modified to treat 3-D cavitating hydrofoils and propellers (Kinnas & Fine, 1993; Fine & Kinnas, 1993; Young & Kinnas, 2001). In Young & Kinnas (2003a,b; 2004), the 3-D BEM was extended to predict the performance of fully-submerged supercavitating hydrofoils and propellers, as well as partially-submerged propellers in spatially varying flow. Most recently, the 3-D BEM was fully coupled with a 3-D finite element method (FEM) to predict the transient hydroelastic response of fully submerged and partially submerged propellers in spatially varying flow (Young,

2007; Young & Shen, 2007; Young, 2008; Young & Savander, 2011).

The 3-D BEM is based on a potential-based formulation for the perturbation flow field. The total inflow velocity is assumed to be composed of the effective inflow velocity (which includes the vortical interaction between the inflow and the structure) and the perturbation potential velocity introduced by the presence of the structure. Hence, the perturbation flow field can be assumed to be incompressible, inviscid, and irrotational. Consequently, the problem can be formulated as a mixed moving boundary value problem of the perturbation velocity potential governed by the Laplace equation. The mixed boundary value problem is solved via a 3-D BEM by applying Green's third identity in the time domain.

The integral surfaces are approximated with hyperboloidal panels (Kinnas & Hsin, 1992) on which piecewise constant strength dipoles and sources are distributed. The flow tangency condition is applied at the wetted blade/foil surface. Only sheet cavitation/ventilation is considered. The pressure on the cavity surface is required to be constant and equal to the saturated liquid vapor pressure for fully submerged cavities, and equal to the atmospheric pressure for ventilated cavities. Viscous effects are considered by applying a constant friction coefficient over the wetted foil/blade surfaces.

To efficiently model the effect of the non-zero trailing edge thickness using the BEM, the base pressure of the hydrofoil is assumed to be constant and equal to P_c. Thus, the extent and thickness of the separated region can be solved like an additional cavitation bubble. This assumption is valid for FA and TR regimes when the foil is base cavitating or base ventilated, and in the SC/FV flow regimes, as long as the cavity pressure, P_c, is known. To avoid "openness" at the foil trailing edge, a small initial closing zone is used. The precise geometry of the initial closing zone is not important, as long as it is inside the separated region and its trailing edge lies on the aligned wake sheet. The original foil section and the closing zone are modeled as one solid body that does not change with time; the size and extent of the cavities and separated region are determined as part of the solution, and hence are allowed to change with time. Details of the formulation and validation for the treatment of supercavitating blade sections can be found in Young & Kinnas (2003a,b; 2004).

To account for the effect of the free surface, the negative image method (Young & Kinnas, 2003a,b & 2004; Young & Savander, 2011) can be applied, but it is ignored in the present calculation because its effect is should be limited for the cases shown, and because the potential is zero at the free surface. Nevertheless, the authors are in the process of implementing the negative image method for SP hydrofoils and the results will be shown at the conference.

3 PHYSICAL MODEL

The SP hydrofoil of interest is shown in Fig. 2(a). It was designed to lift a high-speed unmanned surface vessel (USV) above the water to minimize drag at very high speeds. As explained in Brizzolara et al. (2011) and Brizzolara & Young (2012), the hybrid SWATH, shown in Fig. 2(b), was designed (Brizzolara, 2011) to take advantage of the excellent sea keeping ability of a SWATH for low-speed operations and the superior hydrodynamic efficiency of SP hydrofoils at very high speeds. The design requirements for the USV include the ability to loiter and maintain good seakeeping at low speeds, and to reach a top speed of 120 knots in sea state two. The concept vessel and some of its innovative components have a patent pending.

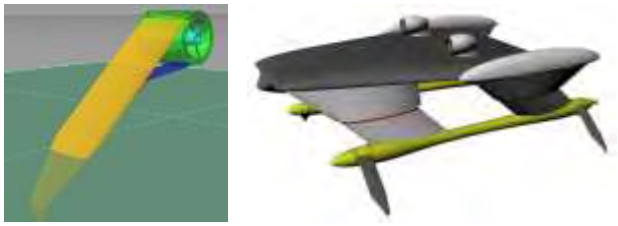

(a) (b)

Fig. 2: Graphical illustration of (a) the SP hydrofoil and (b) the hybrid USV.

For speeds above 60 knots, cavitation is unavoidable. Hence, supercavitating (SC) cross-sections are used to promote supercavitation, where the cavities collapse downstream of the foil trailing edge. Traditionally, SC cross-sections are characterized by a sharp leading edge and a thick trailing edge. These leading and trailing edge characteristics allow the foil to efficiently cut through the water, provide sufficient structural integrity, and encourage the formation of long, thin, and stable gas and/or vapor filled supercavities that extend well beyond the foil trailing edge. However, as explained in Brizzolara (2011) and Brizzolara & Young (2012), traditional SC profiles are very inefficient at low speeds due to separated flow behind the thick trailing edge. To improve the efficiency of SC sections in fully wetted and partially cavitating conditions, a new hybrid section was proposed in Brizzolara (2011) and Brizzolara & Young (2012). The new sectional geometry, along with the plan view of the model-scale SP hydrofoil and experimental setup inside the cavitation tunnel are shown in Fig. 3. The hybrid SC features a classic Johnson three terms profile connected with a strategically shaped annex at the trailing edge through two cusped points to provide good efficiency at low and high speeds, and to control the detachment location of base cavitation at intermediate speeds. The span-wise distribution of camber and angle of attack has been designed with a preliminary version of a lifting line method, specifically reformulated to account for the nonlinear relationship between lift and angle of attack for supercavitating (or ventilated) sections. Recently, the method has been enhanced to account for

dihedral angles with the free surface and winglets (Vernengo & Brizzolara). As demonstrated in Brizzolara (2011) and Brizzolara & Young (2012), the new section is able to yield good efficiency in both low and high speeds.

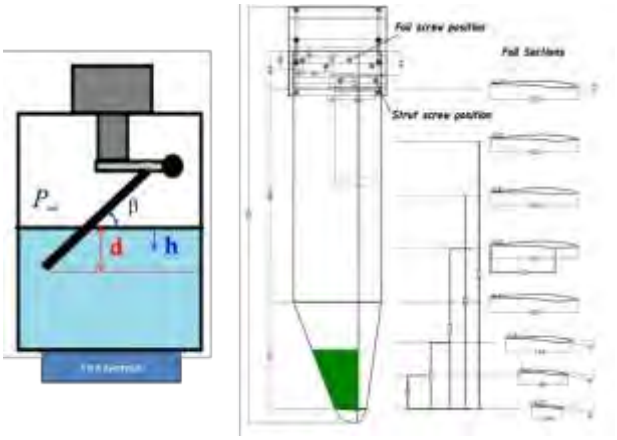

Fig. 3: Graphical illustration of the foil setup up inside the cavitation tunnel viewed from the upstream direction, and plan view of the 1/6-scaled SP hydrofoil geometry.

A 1/6-scaled model of the SP hydrofoil, as shown in Fig. 3 was tested at the free-surface cavitation tunnel at the Technical University of Berlin (TUB). The SP hydrofoil is designed to operate at a dihedral angle of β=40°. It has a trapezoidal planform around the design submergence for high speed operations, and a rectangular planform above for low speed operations. The small winglet at the tip of the foil is used to reduce the induced rag and reduce the shock entry of the foil into the water at low speeds (Brizzolara & Young, 2012). Details of the experimental setup, data, and discussion of the results are given in Brizzolara (2011) and Bizzolara & Young (2012). The test conditions included variations in angle of attack, submergence, tunnel pressure, as well as inflow speed.

4 RESULTS

In this paper, results are shown for the lowest submergence only, where the submerged span, excluding the winglet, is h_o=110 mm and the submerged depth is $d=h_o\sin\beta$. In the BEM discretization, only the submerged portion highlighted in green in Fig. 3 is modeled; the winglet is ignored as it has negligible influence on the lift coefficient; the annex section aft of the two cusp points are approximated as the closing zone, which is inside the cavity and does not affect the performance because it is inside the vaporous or ventilated cavity.

In the BEM model, the pressure on the cavity surface is assumed to be known and is equal to P_c. The local cavitation number, σ, is defined as follows:

$$\sigma = \frac{P_\infty + \rho g h - P_c}{0.5\rho V^2} = \underbrace{\frac{P_\infty - P_c}{0.5\rho V^2}}_{\sigma_c} + \frac{2gh}{V^2} = \sigma_c + \frac{2}{F_h^2}$$

$$\sigma_c = \underbrace{\frac{P_\infty - P_v}{0.5\rho V^2}}_{\sigma_v} - \underbrace{\frac{P_c - P_v}{0.5\rho V^2}}_{\sigma_\Delta} = \sigma_v + \sigma_\Delta \qquad (1)$$

$$F_h = \frac{V}{\sqrt{gh}} = \underbrace{\frac{V}{\sqrt{gd}}}_{F_d}\sqrt{\frac{d}{h}} = F_d\sqrt{\frac{d}{h}}$$

where P_∞ is the atmospheric pressure in full-scale and is the tunnel pressure in model-scale; ρ is the water density; g is the gravitational constant; h is the local submerged depth from the free surface, as shown in Fig. 3; and V is relative inflow velocity. On the cavity surface, $-Cp=(P-P_\infty)/(0.5\,\rho V^2)=\sigma$, which increases with h as shown in Eq. (1). σ_c is the cavity pressure based cavitation number, which does not include the hydrostatic component ($2/F_h^2$). F_h is the local submerged depth (h) based Froude number, and F_d is the total submerged depth (d) based Froude number. σ_v is the vapor pressure (P_v) based cavitation number, and is what is specified during the cavitation tunnel tests by prescribing P_∞ and V. σ_Δ is the differential cavitation number due to differences between P_c and P_v. The cavity behavior is characterized by the following three regimes:

1. If $P_c=P_v$, then $\sigma_\Delta=0$ and $\sigma_c=\sigma_v$, i.e. the cavity is fully vaporous and is closed to the free surface.
2. If $P_c=P_\infty$, then $\sigma_\Delta=\sigma_v$ and $\sigma_c=0$, which occurs when the cavity is fully open to the free surface, the total submergence d is very shallow, and the inflow speed V is very high, i.e. as $F_d\rightarrow\infty$ and $\sigma_v\rightarrow 0$.
3. If $P_v<P_c<P_\infty$, then $\sigma_\Delta>0$ and $0<\sigma_c<\sigma_v$, which occurs when the cavity is open to the free surface at moderate speeds or at deeper submergence.

As noted by Wadlin (1959) and Elata (1967), in order for air to be drawn down to the cavity, $P_c\leq P_\infty$, and can be approximated as follows:

$$P_c - P_\infty \quad 2\rho_a V_a \qquad (2)$$

where ρ_a is the air density and V_a is the air velocity in the throat of the cavity at the free surface. As observed in the experimental studies presented in Wadlin (1958,1959) and Breslin & Skalak (1959), spray sheets are observed around SP hydrofoils/struts, which form the mouth of the ventilated cavity. Since the pressure inside the cavity must be lower than P_∞, and the pressure outside is equal to P_∞, the resulting pressure differential will act to bring the spray sheets together, which will reduce the area at the

mouth of the cavity and accelerate V_a until a dynamic equilibrium is achieved. For a given speed and angle of attack, the shape of the spray sheets, the area at the mouth of the cavity, and hence V_a and P_c, depend on the σ_v and the F_d. Reynolds effect is also expected to important for separation induced ventilation, and Weber number may also play a role because it controls the thickness of the spray sheet and influence free surface rupture. In addition, P_c is influenced by hysteresis effects (Scherer & Auslaender, 1965), as disturbances and air entrainment from previous events will affect the cavity pressure.

Since P_c was not measured in the experiment and it depends heavily on the operating condition and history, σ_c was simply varied between 0 and σ_v in the BEM model to quantify the limits of the performance envelop. The BEM predictions obtained using different σ_c values are compared with experimental measurements in Fig. 4.

To avoid over-crowding the graphs, results are shown for $F_d=V(gd)^{0.5}=10.8$ only. In Fig. 4, $C_L=L/(0.5\rho V^2 A_s)$ is the 3-D lift coefficient, where L is the lift force and A_s is the submerged area, and α is the angle of attack. It should be noted that the lift is positive even at $\alpha=-3^o$ because of the high initial twist angle, as shown in Fig. 3.

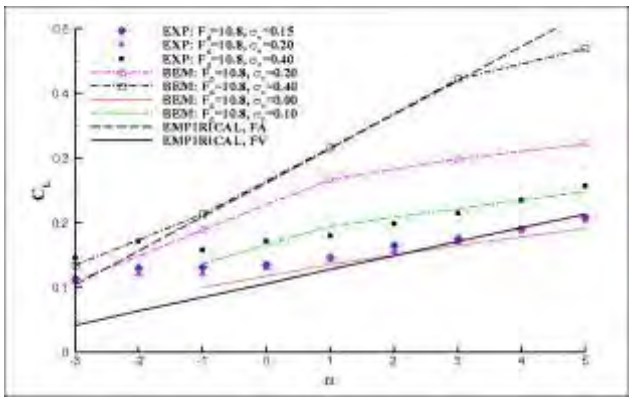

Fig. 4: Comparison of the measured and predicted variation of the lift coefficient with angle of attack. h_o=110 mm and F_d=10.8. Also shown are the empirical lift coefficients for fully attached (FA) and fully ventilated (FV) flow conditions following Frisma (1963).

Figure 4 shows that the measured values are approximately the same for σ_v=0.15 and 0.20, and they both agree with the BEM predictions obtained using σ_c=0.0, which suggest that the Froude number is high enough and the vapor pressure based cavitation number is low enough such that the flow is fully ventilated and $P_c \approx P_\infty$. This is supported by the photographs shown on the top row of Fig. 5 for σ_v=0.20 and F_d=10.8. It should be noted that the photographs are practically indistinguishable between σ_v=0.15 and 0.20, and hence results are only shown for σ_v=0.20. The photographs show that at σ_v=0.20 and α=-3°, the flow is base cavitating except at the winglet (the black portion without the painted white grid), which is fully ventilated (as evident via the more transparent color of the ventilated cavity compared to the more milky white color of the vaporous cavity) due to air drawn through the tip vortex or gas bubbles accumulated from previous runs. As α increases, the ventilated cavity expands upward. At σ_v=0.20 and $\alpha=-1^o$, a very thin (1 grid thick) section of the foil immediately below the free surface is still base cavitating, but the rest of the foil is fully ventilated. The switch from TR to FV flow regimes explains the change in slope around $\alpha=-1^o$ for σ_v=0.15 and σ_v=0.20 observed in Fig. 4. For σ_v=0.15 and 0.20 with $\alpha>-1^o$, the entire foil is fully ventilated, which explains the close agreement of the measured C_L with the BEM predictions obtained using σ_c=0.0.

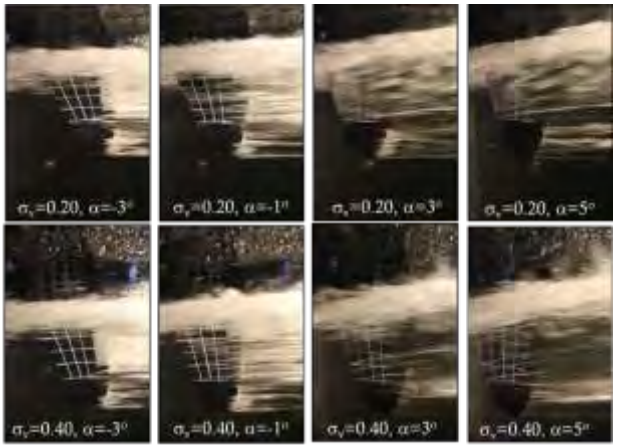

Fig. 5: Selected photographs from model tests the free surface cavitation tunnel at TUB. h_o=110 mm, F_d=10.8.

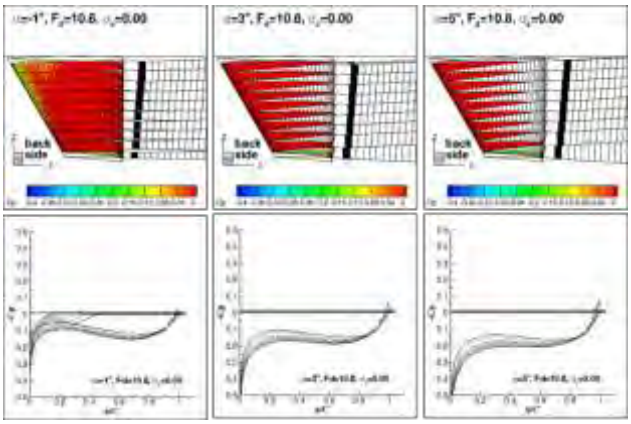

Fig. 6: Predicted cavity pressure distribution and cavity patterns σ_c=0.0, h_o=110 mm, F_d=10.8.

The results shown in Figs. 4 and 5 for $\sigma_v \leq 0.20$ also agree with the predicted pressure distributions and cavitation patterns shown in Fig. 6 for σ_c=0.0 at F_d=10.8. As α increases, the thickness of the suction side ventilated cavity increases; the resulting C_L also increases due to small increases in the pressure on the pressure side, which explains the mild slope of the C_L shown in Fig. 4. For $\alpha<-1^o$, the predicted and measured C_L did not agree as well because the BEM results suggest that part of the suction side is wetted (the ventilated cavities detach from around midchord), and that the leading edge portion of the pressure side is cavitating. It should be noted that no

pictures were taken from the pressure-side during the experiment, and hence the existence of pressure-side cavitation cannot be confirmed. Nevertheless, the photographs in Fig. 5 suggest that the differences may be attributed to the expansion of the ventilated cavity from the winglet due to the very shallow submergence.

The results in Fig. 4 show that for σ_v=0.40 and $\alpha \leq -2^o$, the measured C_L values match well with the BEM predictions with σ_c=0.40, suggesting the cavity is closed to the free surface and $P_c=P_v$. This is supported by the photograph shown on the lower left hand corner of Fig. 5, which shows that the foil is base cavitating except at the winglet. The predicted pressure distribution and cavitation pattern shown on the left column of Fig. 7 for σ_c=0.40 and α=-3^o also show that the flow is based cavitating, and hence the good agreement between the measured and predicted values since $\sigma_c=\sigma_v$. For σ_v=0.40 and $\alpha=-1^o$, most of the foil become fully ventilated except for a thin (one grid thickness) layer immediately below the free surface. For σ_v=0.40 and $\alpha>-1^o$, all of the foil becomes fully ventilated, and the measured C_L for σ_v=0.40 agrees better with BEM prediction with σ_c=0.10. This is because at the higher σ_v, the difference between the P_∞ and P_v is greater, which makes $P_c<P_\infty$ due the reduction in pressure caused by the air flow into the cavity. The good agreement between the measured C_L for σ_v=0.40 and the predicted C_L for σ_c=0.10 suggest that $Pc \approx (3P_\infty - P_v)/4$.

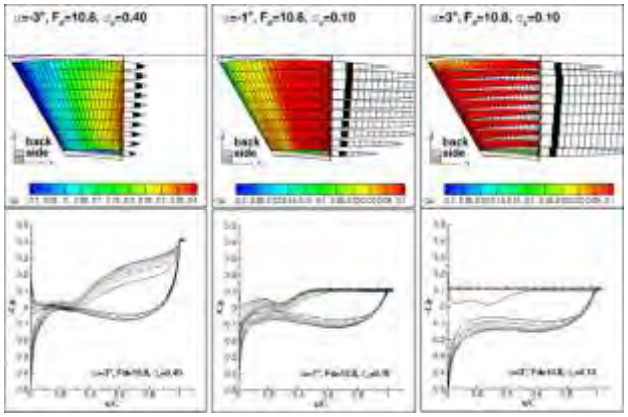

Fig. 7: Predicted pressure distribution and cavity patterns for σ_c=0.40 (left) and σ_c=0.10 (middle and right), h_o=110 mm, F_d=10.8.

The results in Fig. 4 show that the upper limit of the measured C_L match well with BEM predictions for $P_c=P_v$ (FA regime), and the lower limit matched well with numerical predictions for $P_c=P_\infty$ (FV regime). To further verify the results, empirical estimates of C_L for dihedral SP hydrofoils following Frisma (1963) are also shown in Fig. 4. The empirical estimates of C_L for the FA and FV regimes are obtained using Eqs. (3) and (4), respectively.

$$C_{L'}^{FA} = 2\pi(\alpha - \alpha_{Lo}),\ C_L^{FA} = C_{L'}^{FA} / \gamma^{FA}$$
$$\gamma^{FA} = \frac{C_{L'}^{FA}}{C_L^{FA}} = \frac{E}{F} + \frac{K\cos\beta}{2A_R}$$
$$E = \frac{A_R+1}{A_R},\ F = \frac{1-\tan^{-1}\left(2\sqrt{2}\,\frac{h_o}{c}\right)}{4\sqrt{2}\,\frac{h_o}{c}},\ K = 2\left(1-\frac{\beta^o}{75^o}\right) \quad (3)$$

$$C_{L'}^{FV} = \frac{\pi}{2}(\alpha - \alpha_{Lo}),\ C_L^{FV} = C_{L'}^{FV} / \gamma^{FV}$$
$$\gamma^{FV} = \frac{C_{L'}^{FV}}{C_L^{FV}} = \frac{2A_R+1}{2A_R} \quad (4)$$

where the superscripts "FA" and "FV" denote the fully attached and fully ventilated flow regimes, respectively. α_{Lo} is the zero lift angle of attack, γ is the 2-D to 3-D lift coefficient ratio, A_R is the aspect ratio, and c is taken as the effective chord length at the free surface. For h_o=110 mm, $\alpha_{Lo}=-5^o$, A_R=1.32, and h_o/c=1.32.

Application of Eq. (3), which assumes the slope of the 2-D lift curve to be 2π, gives E=0.82 (edge correction factor), F=1.56 (depth correction factor), and K=0.93 (induced drag factor), and γ^{FA}=2.09. Application of Eq. (4), which assumes the slope of the 2-D lift curve to be π/2, gives γ^{FV}=1.28.

As shown in Fig. 4, the BEM predictions obtained using σ_c=0.0 are in good agreement with the empirical estimates for the FV regime, and both are in close agreement with the measured values for $\sigma_v \leq 0.2$ and $-2^o < \alpha < 5^o$. In addition, the BEM predictions obtained using σ_c=0.4 are in good agreement with the empirical estimate for the FA regime, which is also in close agreement with the measured values for σ_v=0.4 and $\alpha \leq -2^o$.

5 CONCLUSIONS

A 3-D BEM previously developed for propellers have been extended for the analysis of a SP hydrofoil, which was designed to support a super high speed unmanned surface vessel. To validate the numerical predictions, results are compared with experimental measurements of a SP hydrofoil tested at the free surface cavitation tunnel of the Technical University of Berlin. The results show that the behavior of a SP hydrofoil is characterized by three flow regimes: fully attached (FA), transitional (TR), and fully ventilated (FV). In the FA regime, the flow was observed to be base cavitating, where $P_c=P_v$. In the TR regime, the flow is very unstable with mixed partial cavitation and/or ventilation patterns. In the FV regime, the cavity is open to the free surface, and $P_v \leq P_c \leq P_\infty$ depending on the operating conditions and hysteresis effects, which leads to large variations in the hydrodynamic load coefficients. The unknown P_c also makes numerical modeling very challenging. Nevertheless, the results show good agreement between measured and predicted values on the upper limit of C_L,

which corresponds to the case when $P_c=P_v$ (fully attached or base cavitating regime), and on the lower limit of C_L, which corresponds to the case when $P_c=P_\infty$ (fully ventilated regime at very high Froude number and very low absolute ambient pressure).

6 FUTURE WORK

The studies presented in this paper highlight the complex hydrodynamic response of a SP hydrofoil, particularly when operating in the TR and FV flow regimes. The results show that the hydrodynamic loads vary significantly with P_c, and hence should be measured in future experimental studies. The authors are in the process of conducting another set of experimental studies to systematically quantify the influence of Froude number, vapor pressure based cavitation number, angle of attack, and submergence on the hydrodynamic response on a newly designed SP hydrofoil. The new hydrofoil has been designed with a new optimized set of design and parametric optimization tools for the shape of the base 2D SC profiles using a combination of surface panel method and a modified lifting line method (Vernengo & Brizzolara, 2011). The goal of the new test series is not only to quantify the mean response, but also the load fluctuations and frequencies. The amplitude of the load fluctuations are expected to be large in the TR flow regime, and it may lead to unwanted vibrations if the excitation frequency matches with the flutter or natural frequencies.

ACKNOWLEDGEMENTS

The authors are grateful to the Office of Naval Research (ONR) and ONR Global for their financial support through grant nos. N62909-10-1-7116, N00014-11-1-0849, and N00014-12-0837 managed by Dr. Robert Brizzolara.

REFERENCES

Breslin, J.P. and Skalak, R. (1959). Exploratory Study of Ventilated Flows about Yawed Surface-Piercing Struts." National Aeronautics and Space Adminstration, NASA MEMO 2-23-59W, Washington, April, 1959.

Brizzolara S. (2011). ONR USV HY2-SWATH. Hydrodynamic Design and Assessment by CFD Methods of HYbrid HYdrofoil / SWATH hulls for a Super High Speed USV. Final report of ONR grant # ONRG-N62909-10-1-7116.

Brizzolara, S., Bovio, M., Federici, A., Vernengo, G. (2011). 'Hydrodynamic Design of a Family of Hybrid SWATH Unmanned Surface Vehicles.' 11th International Conference on Fast Sea Transport. Honolulu, HI, USA, Sept. 26-29, 2011.

Brizzolara, S. and Federici, A. (2011). 'Super-Cavitating Profiles for Ultra High Speed Hydrofoils: a Hybrid CFD Design Approach.' 9th Symposium on High Speed Marine Vehicles, Naples, Italy.

Brizzolara, S. and Young, Y.L. (2012). 'Physical and Theoretical Modeling of Surface-Piercing Hydrofoils for a High-Speed Unmanned Surface Vessel.' 31th International Conference on Ocean, Offshore and Arctic Engineering (OMAE 2012), Rio de Janeiro, Brazil, June 10-15, 2012.

Brizzolara S., Villa D. (2012). Three Phase Ranse Calculation for a Surface Piercing Supercavitating Hydrofoil. Proceedings of the Eighth International Symposium on Cavitation (CAV 2012), August 14-16, 2012, Singapore, Research Publishing Services. ISBN: 978-981-07-2826-7, doi:10.3850/978-981-07-2826-7 084

Elata, C. (1967). 'Choking of Strut-Ventilated Foil Cavities.' Hydronautics, Inc., Technical Report 605-2, Laurel, MD, May, 1967.

Fine, N. and Kinnas, S. (1993). 'A Boundary Element Method for the Analysis of the Flow around 3-D Cavitating Hydrofoils.' Journal of Ship Research. 37: 213-224.

Fridsma, G. (1963). 'Ventilation Inception on a Surface-piercing Dihedral Hydrofoil with Plane-face Wedge Section.' Stevens Institute of Techonlogy, Report No. 952, Hoboken, NJ, October, 1963.

Kinnas, S. and Fine, N. (1991). 'Nonlinear Analysis of the Flow around Partially or Super-cavitating Hydrofoils by a Potential Based Panel Method.' Proceedings of the Boundary Integral Methods – Theory and Applications, IABEM-90 Symposium, Rome, Italy.

Kinnas, S. and Fine, N. (1993). 'A Numerical Nonlinear Analysis of the Flow around Two- and Three-dimensional Partially Cavitating Hydrofoils.' Journal of Fluid Mechanics. 254: 151-181.

Kinnas, S. and Hsin, C.-Y. (1992). 'A Boundary Element Method for the Analysis of Unsteady Flow around Extreme Propeller Geometries.' AIAA Journal. 30(3): 688-696.

Rood, E.P. Jr. and Dialey, N.L. (1973). 'Catastrophic Hydroelastic and Side Vnetilation Phenomena on High-speed Hydrofoil Struts.' Naval Ship Research and Development Center, Report No. SPD-479-10, Bethesda, MD, March 1973.

Scherer, J.O. and Auslaender, J. (1965). 'Experimental and Theoretical Performance of a Supercavitating Hydrofoil Operating near a Free Surface.' Journal of Aircraft. **2**, pp.144-152.

Swales, P.D., Wright, A.J., McGregor, R.C., and Rothblum, R. (1974). 'The Mechanism of Ventilation Inception on Surface Piercing Foils.' Journal of Mechanical Engineering Science, **16**, pp.18-24.

Vernengo G., Brizzolara S. (2012). A Reformulated Lifting Line Theory for Supercavitating Hydrofoil Design. Proceedings of the Eighth International Symposium on Cavitation (CAV 2012), August 14-16, 2012, Singapore, Research Publishing Services. ISBN: 978-981-07-2826-7, doi:10.3850/978-981-07-2826-7 281

Wadlin, K.L. (1958). Mechanics of Ventilation Inception. Second Symposium on Naval Hydrodynamics, Washington, D.C., August 25-29, 1958.

Wadlin, K.L. (1959). Ventilated flows with Hydrofoils. Twelfth General Meeting of the American Towing Tank Conference, University of California, Berkley, CA, August 31-September 2, 1959.

Waid, R.L. (1968). 'Experimental Investigation of the Ventilation of Vertical Surface-Piercing Struts in the Presence of Cavitation'. Lockheed Missiles & Space Company, Report No. LMSC/D019597, Sunnyvale, CA, May 1968.

Young, Y.L. and Kinnas, S.A. (2001). 'A BEM for the Prediction of Unsteady Midchord Face and/or Back Propeller Cavitation.' Journal of Fluids Engineering. 123: 311-319.

Young, Y.L. and Kinnas, S.A. (2003a). 'Analysis of Supercavitating and Surface-Piercing Propeller Flows via BEM.' Computational Mechanics. 32(5-6): 269-280.

Young, Y.L. and Kinnas, S.A. (2003b). 'Numerical Modeling of Supercavitating Propeller Flows.' Journal of Ship Research, 47: 48-62.

Young, Y.L. and Kinnas, S.A. (2004). 'Performance Prediction of Surface-Piercing Propellers.' Journal of Ship Research. 28(4): 288-305.

Young, Y.L. and Shen. Y. (2007). 'A Numerical Tool for the Design/Analysis of Dual-Cavitating Propellers.' Journal of Fluids Engineering. 129(6): 720-730.

Young, Y.L. (2007). 'Time-Dependent Hydroelastic Analysis of Cavitating Propulsors.' Journal of Fluids and Structures. 23: 269-295.

Young, Y.L. (2008). 'Fluid-Structure Interaction Analysis of Flexible Composite Marine Propellers.' Journal of Fluids and Structures. 24: 799-818.

Young, Y.L. and Savander, B.R. (2011). 'Design, Analysis, and Challenges of Large-Scale Surface-Piercing Propellers.' Ocean Engineering. 38: 1368-1381.